

Article

Integrating Transparent and Conventional Solar Cells TSC/SC

Moh'd Al-Nimr, Abdallah Milhem , Basel Al-Bishawi and Khaleel Al Khasawneh * 

Department of Mechanical Engineering, Jordan University of Science and Technology, Irbid 22110, Jordan; malnimr@just.edu.jo (M.A.-N.); abdullahmelhem007@gmail.com (A.M.); baselbishawi@yahoo.com (B.A.-B.)

* Correspondence: krkhasawneh@just.edu.jo

Received: 11 August 2020; Accepted: 7 September 2020; Published: 11 September 2020



Abstract: Conventional photovoltaic cells are able to convert the visible light spectrum of solar radiation into electricity; the unused wavelengths of the solar radiation spectrum are dissipated as heat in the system. On the other hand, certain types of transparent solar cells are able to utilize the rest of the solar radiation spectrum. The integration of transparent solar cells with conventional photovoltaic cells enables the system to absorb and utilize both wavelengths of the solar radiation spectrum. In this paper, two models for integrating transparent solar cells with conventional photovoltaic cells are proposed, simulated, and analyzed theoretically. ANSYS software was used to obtain the results for the proposed models. It is an initial theoretical study that shows some first results; it is almost a work in progress. The results showed that the highest efficiency was for the model that had two cooling spaces. The efficiency was increased as the ambient air temperature decreased and the mass flow rate increased. The percentage drop in photovoltaic (PV) cell efficiency decreased as the mass flow rate increased and the ambient temperature decreased, and it had the lowest value when air/water was used for cooling. The efficiency of the transparent solar cell (TSC) increased as the transparency decreased; in order to have higher efficiency, PV efficiency should be high, with low transparency. When added, the transparent solar cell was supposed to increase the harvested energy due to the utilization of the unconverted solar radiation, but it left two negative side effects. The first negative side effect was the reduction of the transmitted radiation to the conventional solar cell due to the transmissivity of the transparent cell. The second negative impact was the increase in the conventional cell temperature due to the additional thermal resistance, which reduced the effectiveness of cooling the cell from above. The proposed models were verified by comparing the results of the standalone PV that were available in the literature with the two models that are proposed in this paper.

Keywords: transparent solar cell; integrating cell; efficiency; photovoltaic cell

1. Introduction

Energy harvesting is considered a mutual interest nowadays. Harvesting the energy that solar radiation possesses is one of the most important fields of energy harvesting. Solar radiation has three main parts: 46% visible light with a wavelength of 380 to 750 nm, 47% infrared light (IR) with a wavelength of 750 to 1 mm, and 7% ultraviolet light (UV) with a wavelength from 10 to 380 nm [1]. Both IR and UV light are generally invisible to human eyes. In past years, scientists have come up with several ways to harvest the energy of light, where the most efficient way is solar cells. Those solar cells convert the light's energy to electrical energy by allowing photons of light to knock electrons free from atoms to generate electricity [2]. The unused wavelengths (ultraviolet and infrared) do not have enough energy to dislodge the electrons and are absorbed by the system as a loss. This part of the energy can be utilized by integrating transparent solar cells with conventional photovoltaic cells that enable the system to absorb both wavelengths of the solar radiation spectrum.

Any conventional photovoltaic (PV) cell is able to convert certain wavelengths of solar radiation into electricity with a certain efficiency. As such, scientists have continuously tried continuously to increase the efficiency of PV cells in various ways. One of these ways is using different materials in the cell. The first solar cell was introduced by Charles Fritts in 1883 using selenium on a thin layer of gold, with an efficiency of less than 1%. The first practical silicon solar cell was announced by Bell Labs in 1954, with an efficiency of 6%.

There are many types of PV cells that have been developed over the years; the oldest one is the monocrystalline silicon PV cell. In this cell, a thin layer of pure silicon crystal is used, and it is capable of converting up to 26% of the light's energy. However, in the past, it had a high initial cost, as well as poor aging properties [3]. Moreover, the polycrystalline silicon PV cell had higher durability and a lower initial cost. It used thin plates of solidified silicon, which has many impurities that make it possess slightly lower efficiencies (within a range of 12%). Additionally, it is known as polysilicon and multisilicon. Furthermore, hydrogenated silicon is one of the alternatives for a PV cell, but this type has particularly low efficiency due to a thinner absorbing layer and light degradation issues [4,5]. When it comes to the world market, cadmium telluride is placed second after the crystalline silicon; it represents 5% of the world's market due to its low production cost compared to other types. It has a laboratory efficiency of 22.1%; however, its commercial module has an efficiency of 16.1% [6]. Eventually, scientists succeeded in reaching an efficiency of 29% by using a compound of gallium and arsenide with a few micron layer thickness; however, it is considered to be an expensive material.

Despite the continuous studies to increase the efficiency of different PV cells, there is always one challenge regarding the cooling of the PV. PV devices can lose up to 0.5% of their maximum power for each 1 °C increase in its temperature. This can cause a long return on investment period, which makes it inefficient. This problem was solved by hybrid PV thermal cells, which introduced water cooling systems. It improved the thermal module's efficiency, but it was complicated and expensive. Different types of cooling techniques have been tried. Some were simple, such as using water and air, and some were based on inductive cooling and phase-change material cooling [7,8]. However, a few years ago, the efficiency of these cells reached around 40% under ideal conditions, but this efficiency dropped to its typical value of around 30% under practical usage. Even though the previous efficiencies are considered relatively high, the main drawback remains that conventional PV cells have the ability to convert only visible light into electricity. This was solved in August 2014 by MIT researchers when they created a fully transparent solar cell (TSC). Transparent solar cells are capable of converting the invisible portion of solar radiation into electricity [9]. A transparent solar cell consists of organic salts, which are complex cyanine derivatives used with glass, unlike traditional solar cells. It allows visible light to pass through, making it possible to see through it. TSCs have an estimated efficiency of 4%, which is still not enough to use by itself. In pure silicon, the electrons have the ability to absorb light that is emitted towards them to move from one place to another (conventional PV cell). However, this is not the case with TSCs, where glass is used. Glass is considered to be silicon dioxide and will not have the same light absorption properties as pure silicon, which means that sun rays will be able to pass through TSCs without getting absorbed [10].

In the literature, there are many papers that have studied the conventional standalone photovoltaic cells, with and without a cooling system. Numerous papers have studied the standalone transparent solar cells experimentally, numerically, and analytically. The TSC simulated experimentally by Suzuoki et al. [11] consisted of layers of polyethylene and ethylene–vinylacetate copolymer (EVA). A comprehensive review of transparent solar photovoltaic technologies is provided by Alaa et al. [12], while Da et al. [13] proposed a comprehensive study to increase full-spectrum solar energy utilization in PV–TE (photovoltaic–thermoelectric) cells. Additionally, Karima et al. [14] modeled and simulated a typical single-pass hybrid photovoltaic/thermal (PV/T) air collector. A comprehensive review of the latest literature on PV power generation was compiled by Hosenuzzaman et al. [15], and Kaiyang et al. [16] presented an analysis of the mechanical properties of transparent conducting oxide, indium tin oxide, and indium zinc oxide thin films on the glass substrates. Shukla et al. [17] provided a detailed design

of a standalone solar PV system. It outlines the detailed procedure for specifying each component of the standalone rooftop solar PV system and its performance analysis using simulation software. Betancur et al. [18] proposed a study for light-harvesting recovery to bring the photon-to-charge conversion up to almost 80% of that of its opaque counterpart.

An overview of the cost analysis of PV cells and their environmental impact was presented by Tyagi et al. [19], while Sarhaddi et al. [20] investigated the thermal and electrical performance of a solar photovoltaic thermal (PV/T) air collector. A detailed thermal and electrical model has been developed to calculate the thermal and electrical parameters of a typical PV/T air collector. Additionally, Parket et al. [21] investigated the electrical and thermal performance of a semitransparent PV module that was designed as a glazing component. A study for the use of reflecting panels with conventional solar collectors and photovoltaic panels was provided by Pucar and Despic [22], while Karthick et al. [23] provided a study for the semitransparent photovoltaic module that is used in glazing materials of the skylights in residential buildings. A hybrid model of a concentrated photo-thermo chemical photovoltaic system was proposed by Wang et al. [24]. Additionally, Schiro et al. [25] presented a study to investigate the possibility of adding a cooling system to existing photovoltaic units without changing the original module structure. Yin et al. [26] proposed a method for a concentration spectrum-splitting photovoltaic-thermoelectric hybrid system. An investigation of the behavior of the solar power generation system that consists of a concentrated photovoltaic/thermal system that utilizes an organic Rankine cycle integrated with a geothermal condenser and an energy storage unit was provided by Al-Nimr et al. [27]. Additionally, Li et al. [28] investigated optimum thermoelectric geometry for the optimum performance of a photovoltaic–thermoelectric device and a solar thermoelectric generator. Manokar et al. [29] introduced a work to study the performance of a PV-panel-integrated solar still. In addition, Osam et al. [30] provided a comparison study between ST and PV solar technologies for industrial applications. Katsura et al. [31] proposed a new, low-cost insulation method using slim transparent panels with structured cores for the windows of existing buildings. Alrashidi et al. [32] investigated experimental semitransparent cadmium-telluride-based BIPV for windows, characterized using outdoor test cells in the temperate UK climate.

Based on this review, it seems that from the authors' viewpoints, no one has studied this new combination of conventional PV cells with TSCs. The objective of this research paper is to introduce a new model of transparent solar cells integrated with conventional photovoltaic cells (TSC/SC) that able to absorb and utilize both wavelengths of the solar radiation spectrum: the ultraviolet, infrared, and visible light spectrum. Two combination systems will be modeled, simulated, investigated, and analyzed, with two different working fluids as a coolant. Air or water will be used as a cooling fluid in order to achieve the highest efficiency. The present results will be compared with the results of conventional photovoltaic cells. This study does not take economic aspects into consideration, and these aspects will be the focus of an upcoming study after commercializing the transparent TSC/SC cell.

2. System Description and Thermal Model

The integrated system of transparent solar cells (TSCs) with conventional photovoltaic cells (PVs) will be able to convert both visible and invisible portions of wavelengths of solar radiation spectrum into electricity. Traditional PV cells are capable of absorbing only 46% of total light energy. Therefore, to achieve more efficiency, several parameters must be taken into consideration, including the efficiency of traditional PV cells and TSCs, the working fluid, TSC transparency, and the space between the TSC and the PV cell. Conventional PV cells deal with visible light, while transparent solar cells convert infrared and ultraviolet light using a certain mechanism.

This combination will affect the overall thermal model efficiency in two ways: first, less radiation will be received by the conventional PV cells since some of the sun rays will be blocked by the TSC, which will reduce the output power compared to the standalone PV. Second, the difficulties of cooling this new system will be a new challenge. As mentioned early, cooling has a massive effect on the efficiency of the PV; this combination can result in the heating of both TSC and PV cells, which will

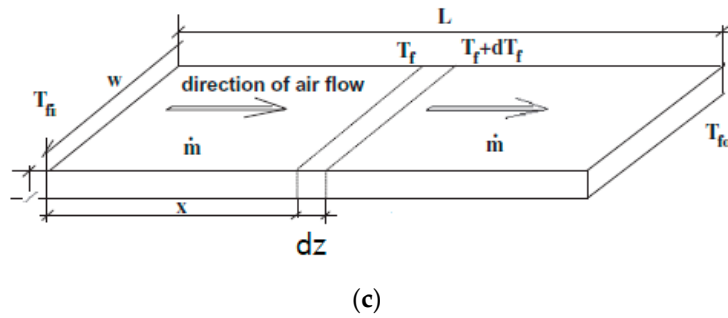


Figure 1. Schematic cross-sectional view of the two models: (a) Model 1; (b) Model 2; (c) an elemental length, dz, of flowing fluid inside the duct.

Allowing air or water to flow between the two solar cells has an essential role in providing the required cooling of the model. This is a very important geometric parameter regarding the efficiency of the TSC and the overall efficiency of the model. The space will play a major role in preventing the overheating of the TSC and the conventional PV cell. As such, this new model of the integration of the PV cell with the TSC can be optimized.

The models were simplified by using electrical analogy regarding conduction, convection, and radiation heat transfer (thermal resistances), as shown in Figures 2 and 3 for Models 1 and 2, respectively. This representation will be exploited in the analysis and the problem-solving.

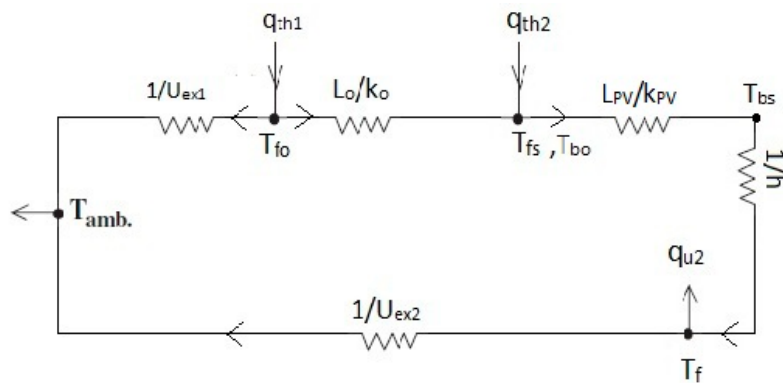


Figure 2. Thermal resistance circuit of Model 1.

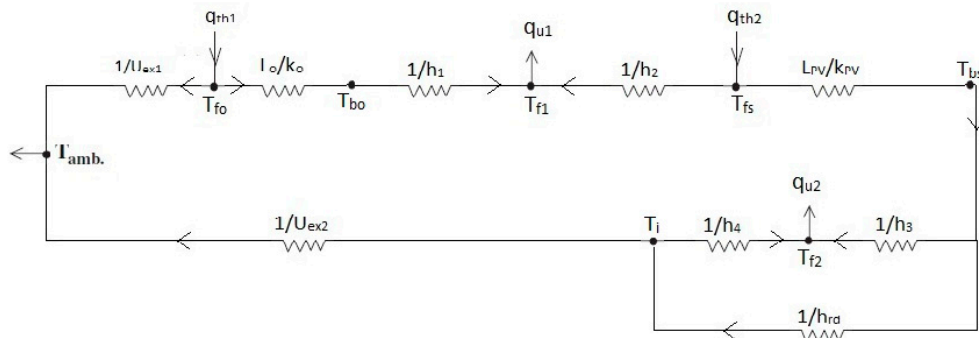


Figure 3. Thermal resistance circuit of Model 2.

Regarding the geometry, both models have a width (W) of 1 m and a length (L) of 2 m. The x-axis is along the width of the model, while the z-axis is along the length of the model and the y-axis is along the depth of the model. The origin of the coordinate system is at the left top of the rear corner of the model. The applied analysis is based on standard conditions, where the solar radiation is assumed to be 1000 W/m² and the velocity of the ambient air is assumed to be 1 m/s. Different values of mass flow

rate inside the duct will be simulated to determine the effect of the velocity of the working fluid on the cooling process and efficiency. All properties have been taken at a temperature of 25 °C.

The modeling and analysis were made based on the following assumptions:

- 1 The thermal model is in steady-state conditions.
- 2 The temperature of the thermal model varies only along the length of the model (one-dimensional analysis); no temperature change along the width of the model.
- 3 The ambient temperature is the same in all directions relative to the model, and the heat losses are only from the model's front and back sides to the ambient air.
- 4 The flow in the duct is incompressible, uniform, steady, and fully developed.
- 5 Flowing fluid has constant properties.
- 6 Forced convection has been taken into consideration only.
- 7 Wind speed is uniform above and below the model.
- 8 Side losses are negligible.

3. Governing Equations and Mathematics

Considering an element of flowing fluid inside the fluid duct of Model 1, with a width of W and a length of dz and by applying the energy balance principle on this element [33], as shown in Figure 1c, then

$$\dot{m}C_p dT_f = Wdz[h(T_{bs} - T_f) - U_{ex2}(T_f - T_{amb})] \quad (1)$$

where \dot{m} is the mass flow rate of the flowing fluid. For Model 1, U_{ex2} is the overall heat transfer coefficient at the bottom of the PV; $U_{ex2} = h_w$ is the convection heat transfer coefficient of the wind at the outside surface of the thermal model since the back of this model is not insulated; C_p is the specific heat capacity of the working fluid; h is the convective heat transfer coefficient from the back surface to the working fluid. For the convection heat transfer coefficient, the relation that was introduced by Ozisik [34] can be used for flow over a flat plate: $h = 0.036 \frac{k}{L} Pr^{0.43} (Re^{0.8} - 9200)$. Where k is the thermal conductivity of the fluid, L is the length of the surface. T_f, T_{bs}, T_{amb} is the temperature of the working fluid, back surface of the PV, and ambient temperature, respectively.

Applying the energy balance principle on each element of the collector of Model 1 yields [35]

$$q_{th1} + q_{th2} = q_u + U_{ex1}(T_{fo} - T_{amb}) + U_{ex2}(T_f - T_{amb}) \quad (2)$$

resulting in

$$q_{th1} + q_{th2} = q_u + (h_{rg} + h_w)(T_{fo} - T_{amb}) + h_w(T_f - T_{amb}) \quad (3)$$

Then

$$q_u = q_{th1} + q_{th2} - (h_{rg} + h_w)(T_{fo} - T_{amb}) - h_w(T_f - T_{amb})$$

Since the bottom surface of the TSC is in contact with the front surface of the PV, then $T_{bo} = T_{fs}$, where T_{fs} is the PV cell's front surface temperature, T_{bo} is the TSC's bottom surface temperature, T_{bs} is the PV cell's bottom temperature, T_{fo} is the organic TSC's front temperature, q_{th1} is the heat generation rate on the surface of the TSC, q_{th2} is the heat generation rate on the surface of the PV cell, q_u is the amount of useful heat removed by the fluid, and U_{ex1} is the overall heat transfer coefficient of the top side, including h_{rg} and h_w .

Applying the energy balance principle on Model 2 results in the following equations [35].

$$T_{fo} = \frac{q_{th1} + T_{bo} \frac{k_o}{L_o} + T_{amb} U_{ex1}}{\frac{k_o}{L_o} + U_{ex1}} \quad (4)$$

$$T_i = \frac{T_{bs}h_{rd} + T_{f2}h_4 + T_{amb}U_{ex2}}{h_{rd} + h_4 + U_{ex2}} \quad (5)$$

where k_o is the thermal conductivity of organic TSC, L_o is the thickness of the organic TSC, T_{f2} is the mean temperature of the fluid inside the lower duct between the bottom of the PV and the insulation material, T_i is the temperature of the insulation material, h_{rd} is the radiation heat transfer coefficient between the bottom of the PV and the surface of the insulation material, and h_4 is the convection heat transfer coefficient at the insulation surface.

Applying the energy balance principle on an element of fluid of Model 2 in the top fluid duct:

$$\dot{m}_1 C_{p1} dT_{f1} = W dz [h_1(T_{bo} - T_{f1}) - h_2(T_{fs} - T_{f1})] \quad (6)$$

Additionally, applying the energy balance principle on an element of fluid of Model 2 in the bottom fluid duct:

$$\dot{m}_2 C_{p2} dT_{f2} = W dz [h_3(T_{bs} - T_{f2}) - h_4(T_i - T_{f2})] \quad (7)$$

where the energy balance on the cell of Model 2 is

$$\begin{aligned} q_{th1} + q_{th2} &= q_{u1} + q_{u2} + U_{ex1}(T_{fo} - T_{amb}) + U_{ex2}(T_i - T_{amb}) \\ q_{u1} + q_{u2} &= q_{th1} + q_{th2} - U_{ex1}(T_{fo} - T_{amb}) - U_{ex2}(T_i - T_{amb}) \end{aligned} \quad (8)$$

where U_{ex1} for Models 1 and 2 is

$$U_{ex1} = h_{rg} + h_w \quad (9)$$

while U_{ex2} for model 2 is

$$U_{ex2} = \left(\frac{L_i}{k_i} + \frac{1}{h_w} \right)^{-1} \quad (10)$$

where \dot{m}_1 is the mass flow rate in the duct between the TSC and the PV; \dot{m}_2 is the mass flow rate in the duct between the bottom of the PV and the surface of the insulation material; T_{f1} is the mean temperature of the fluid inside the upper duct between the front of the PV and the TSC; h_1 is the convection heat transfer coefficient at the bottom of the TSC; h_2 is the convection heat transfer coefficient at the top of the PV; T_{fs} is the PV front surface temperature; q_{u1} is the rate of thermal energy absorbed per unit area of the TSC by the fluid in the upper fluid duct in Model 2; q_{u2} is the rate of thermal energy absorbed per unit area of the PV by the fluid in the lower fluid duct in Model 2; h_{rg} is the radiation heat transfer coefficient between the TSC and the sky. A layer of insulation has been taken into consideration in Model 2.

$$h_w = 2.8 + 3V_w \quad (11)$$

V_w, h_w , is the wind speed and the convection heat transfer coefficient of the wind, respectively [14]. The radiation heat transfer coefficient between the bottom of the PV and the surface of the insulation material is

$$h_{rd} = \sigma \frac{(T_{bs} + T_i)(T_{bs}^2 + T_i^2)}{\frac{1}{\varepsilon_1} + \frac{1}{\varepsilon_2} - 1} \quad (12)$$

where σ is the Stefan–Boltzmann constant, ε_1 is the emissivity of the PV, and ε_2 is the emissivity of the insulation material. Since both of the models will have same h_{rg} , then

$$h_{rg} = \sigma \varepsilon_{TSC} \frac{(T_{fo} + T_{sky})(T_{fo}^2 + T_{sky}^2)(T_{fo} - T_{sky})}{T_{fo} - T_{amb}} \quad (13)$$

where $T_{sky} = 0.0552 T_{amb}^{1.5}$ [14]

According to the solar radiation percentage part, as mentioned above, the solar radiation absorbed by the TSC for Model 1 or 2 is equal to $G(1 - \tau_{TSC}\xi)$, while the part of electrical power that the TSC cell can convert is

$$E_{TSC} = G(1 - \tau_{TSC}\xi)\alpha_{TSC}\eta_{TSC} \quad (14)$$

where ξ the percentage of the visible light, E_{TSC} is the generated electrical power of the TSC, α_{TSC} is the absorptivity of the TSC, τ_{TSC} the transparency of the TSC, and η_{TSC} is the efficiency of the TSC. The remaining part that the TSC unable to convert to electrical power will dissipate as heat in the TSC cell as follows:

$$q_{th1} = G(1 - \tau_{TSC}\xi)(1 - \alpha_{TSC}\eta_{TSC}) \quad (15)$$

The part of the radiation that absorbed by the PV is equal to $G(\tau_{TSC}\xi)$, and the part of the electrical power that the PV cell will convert is

$$P_{PV} = G\tau_{PV}\xi\alpha_{PV}\eta_{PV,eff} \quad (16)$$

$$\eta_{PV,eff} = \frac{\eta_{PV}}{\xi} \quad (17)$$

$$P_{PV} = G\tau_{TSC}\alpha_{PV}\eta_{PV} \quad (18)$$

The other part that the PV cannot convert to electrical power will dissipate as heat in the PV cell.

$$q_{th2} = G\tau_{TSC}(\xi - \alpha_{PV}\eta_{PV}) \quad (19)$$

P_{PV} is the generated electrical power of the PV, α_{PV} is the absorptivity of the PV, τ_{PV} is the transparency of the PV, η_{PV} is the efficiency of the PV cell, and G is the incident solar radiation; the thermal efficiency of the model is [14]

$$\eta_{th} = \frac{\sum Q_u}{GA} \quad (20)$$

where Q_u is the amount of the useful heat, and A is the model surface area.

In order to make sure that the integrated TSC/PV produces more power than the PV alone (under the same incident solar radiation), we intended to find the ranges of TSC transmissivity and efficiency that help in attaining this objective. Hence, to calculate the minimum requirements of TSC efficiency and transparency, the electrical output power of TSC and PV should be summed up and compared with the output electrical of the PV standalone as follows:

$$\alpha_{TSC} \frac{\eta_{TSC}}{\eta_{PV}} + \tau_{TSC} \left(\alpha_{PV} - \xi \alpha_{TSC} \frac{\eta_{TSC}}{\eta_{PV}} \right) = 1 \quad (21)$$

Equations (1)–(3) can be used to calculate the temperature of the surfaces and the cooling fluid along the thermal model (Model 1). In other words, data points can be obtained to generate a relationship between the mass flow rate of the cooling fluid and the surface temperature of the model. The same analysis is used for Model 2 by using Equations (4)–(8). However, Equations (14)–(19) were used to calculate the heat generation within the solar cell and to calculate the output electrical energy of both the TSC and the traditional PV cell in both models. Whereas Equation (20) indicates the thermal efficiency regarding the amount of fluid that can be used for domesticating the purpose, Equation (21) represents the relationship between the PV and TSC efficiencies, which can be used to determine the optimum output between the two cells. Based on Equation (21), optimizing the thermal model can be done through manipulating TSC transparency and thus its efficiency with the PV. Additionally, the relationship between the temperature coefficient of maximum power efficiency is approximated as Karima et al. [14]

$$\gamma = \frac{\eta_{mp,ref}\beta}{V_{pm,ref}} \quad (22)$$

where the subscript mp indicates the maximum power point, β (the voltage temperature coefficient) = -0.077 V/K, and γ (the temperature coefficient of maximum power point efficiency) = 5.6×10^{-4} K $^{-1}$.

$$\eta_{mp} = \eta_{mp,ref} + \gamma(T_c - T_{c,ref}) \quad (23)$$

where $\eta_{mp,ref}$ (the electrical efficiency at maximum power point at reference condition) = 15%, $V_{pm,ref}$ is the output voltage at maximum power point at reference condition (V), T_c the cell temperature(K), and $T_{c,ref}$ (the reference cell temperature) = 298.15 (K) [14]

$$\eta_{mp,ref} = \frac{P_{mp,ref}}{AG} = \frac{I_{mp,ref}V_{mp,ref}}{AG} \quad (24)$$

$I_{mp,ref}$ is the output current at maximum power point at reference condition (A); G reference solar radiation = 1000 (W/m 2).

4. Results and Discussions

ANSYS software was used to obtain the results for the proposed models. The TSC is modeled with the same properties as glass. The PV is modeled with the same material properties as a traditional PV cell: a layer of glass, EVA (ethylene–vinyl–acetate copolymer), and silicon. Table 1 shows the properties of the PV cell and the TSC that are simulated, and Table 2 shows the values of the design parameters that are used for Models 1 and 2, where air and water are used as flowing fluid. The back layer (Tedlar layer) of the PV is excluded from the simulation software due to its small thickness compared to other major parts.

Table 1. Materials properties used in this work.

Material	Density (g/cm 3)	Specific Heat (J/kg.K)	Thermal Conductivity (W/m.K)	Thickness (mm)	Emittance
Insulation	0.160	100.00	0.038	50.0	0.75
Glass (TSC)	2.700	780.33	1.700	3.0	0.88
EVA	0.930	3135.00	0.235	0.8	–
Silicon	2.285	710.08	148.000	0.4	0.85

Table 2. Values of the design parameters for Models 1 and 2 used in this work.

Parameter, (Unit)	Value	Parameter, (Unit)	Value
L, (m)	2	Li (cm)	5
W, (m)	1	Lo (mm)	3
Cooling space depth, Model 1, (mm)	50	Cooling spaces depth, Model 2, (mm)	100
Lpv, (mm)	50	Cp, Air, (kJ/kgK)	1
Vw, (m/s)	1	Cp, Water, (kJ/kg K)	4.18

The first case simulated is the integration of the TSC with the PV without a cooling space. Figure 4 shows a comparison of the simulation result of the standalone PV with the result of Model 1 without cooling. This figure shows extensive overheating of both solar cells since no cooling fluid is allowed to flow between the two solar cells of Model 1. As a result, the forced convective heat transfer is terminated, which results in extremely low efficiency since the voltage will drop linearly. The same result can be concluded for power production as power is generated through the difference in energy for the electrons that exist in the core material. When the solar panel is overheated, then the difference

between solar energy and the remaining energy (solar cell) will be low, which will result in a reduction of output power. This makes Model 1, integrating the TSC with the PV without cooling, inefficient.

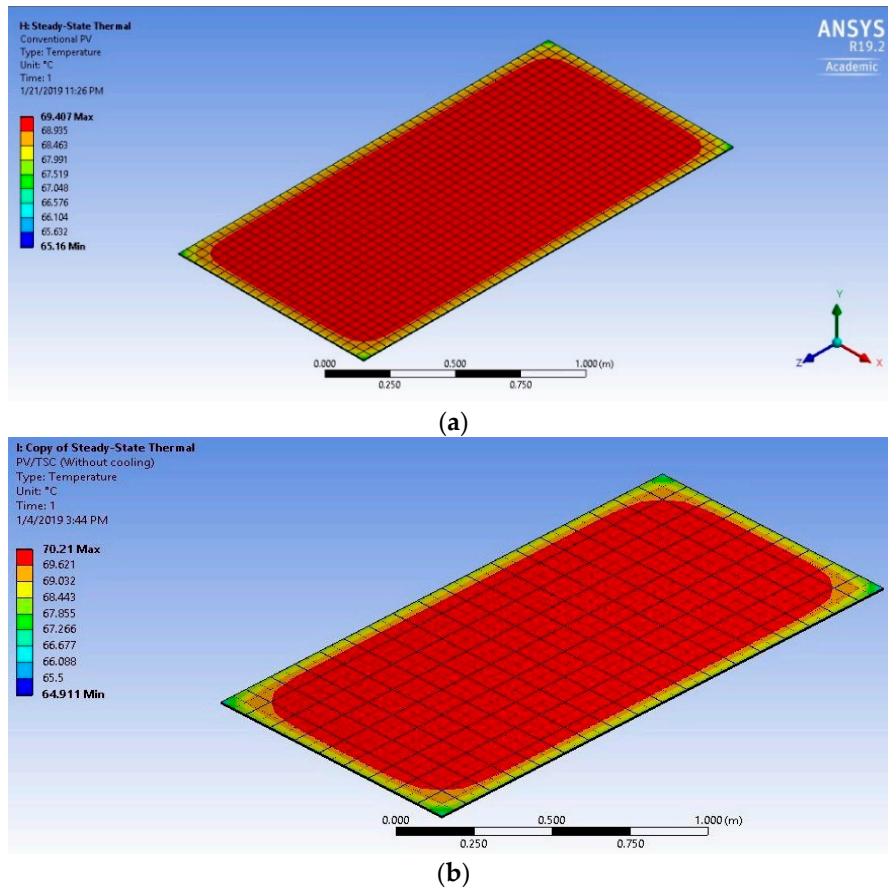


Figure 4. Temperature contours (°C): (a) standalone PV; (b) Model 1 without cooling.

The effect of using air as a cooling fluid inside the duct that is attached below the conventional PV cell for Model 1, with no spacing between the TSC and the PV cell, is shown in Figure 5. It can be observed that the temperature had dropped down but was still not in the operating range.

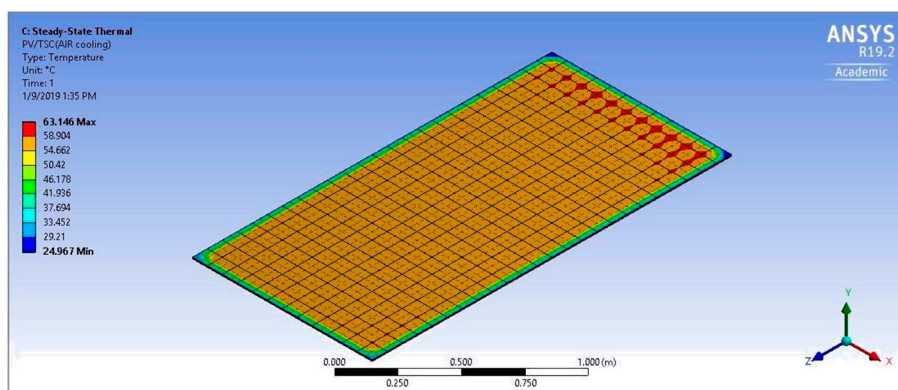


Figure 5. Temperature contours (°C) of Model 1 with air cooling.

Water can be used instead of air inside the duct as a working fluid to improve the cooling process since water has higher heat capacity and a higher convection heat transfer coefficient. Figure 6 shows the contours of the temperature for this case, which is still relatively high and above the optimum

operating temperature. Table 3 shows the maximum and minimum values of the temperature for Model 1 as a comparison with the standalone PV cell. The results provided in this table validate this model.

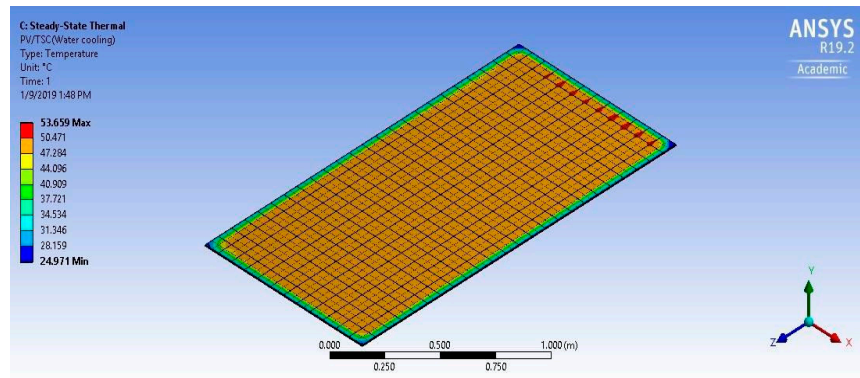


Figure 6. Temperature contours ($^{\circ}\text{C}$) of Model 1 with water cooling.

Table 3. The maximum and minimum temperature of the PV for Model 1. $T_{\max, s \text{ tan dalone}} = 69.50 \text{ }^{\circ}\text{C}$; $T_{\min, s \text{ tan dalone}} = 65.16 \text{ }^{\circ}\text{C}$.

Temperature ($^{\circ}\text{C}$)	Standalone PV, [36].	Without Cooling	Air Cooling	Water Cooling
Max. Temperature ($^{\circ}\text{C}$)	69.45	70.21	63.15	53.66
Min. Temperature ($^{\circ}\text{C}$)	65.10	64.91	24.97	24.97

Another important factor in the cooling process is the ambient temperature. This can directly affect the surface temperature of both solar cells, resulting in lower output power as it becomes high. As such, to study the effect of this parameter in the efficiency of Model 1, a mass flow rate of 0.5 kg/s of the working fluid, with different ambient temperatures, is used for this model. The required TSC efficiency, just to have the same output power as the standalone PV, is shown in Figure 7. To maximize the efficiency of this model, two factors should be satisfied: low ambient temperature and the use of efficient cooling fluid such as water. The worst scenario is without cooling and higher ambient temperatures. Obtaining a low surface temperature for both cells is a very important factor regarding the efficiency of the model. This can be obtained by increasing the flow rate of the fluid inside the bottom duct. The higher the flow rate, the higher the fluid velocity inside the duct and the higher the convection heat transfer coefficient. Figure 8 shows the required TSC efficiency just to have the same output power as the standalone PV, with the same mass flow rate. The same conclusion is valid for the conventional PV since the flow rate will affect the TSC cooling rate, which means it should also affect PV cell efficiency. Additionally, Figure 9 shows the mass flow rate effect in the percentage drop in PV cell efficiency.

The improvement in PV efficiency is represented as the percentage drop in PV efficiency. The percentage drop decreases as the flow rate increases due to the higher heat transfer rate, which means lower surface temperature and better efficiency. It is noted that TSC efficiency is related to conventional PV efficiency since TSC efficiency is dependent on the ambient temperature due to its direct effect on the surface temperature and power production. Therefore, the ambient temperature will affect PV efficiency as well. This trend is shown in Figure 10, and it shows a comparison between Model 1 and the standalone PV cell. This figure shows that Model 1 without cooling is in good agreement with the standalone PV cell, while using a cooling process in this model will improve the results. This figure

shows the validation of the present model since the results of the standalone PV are in good agreement with Model 1 without cooling.

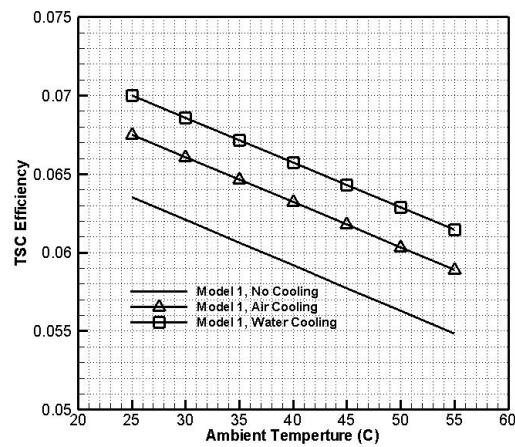


Figure 7. Effect of the ambient temperature in TSC efficiency for Model 1, mass flow rate = 0.5 kg/s.

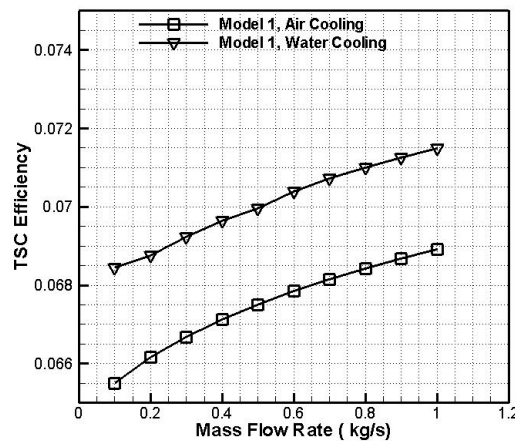


Figure 8. Effect of the mass flow rate of the flowing fluid in TSC efficiency for Model 1. $T_{amb} = 25^{\circ}\text{C}$.

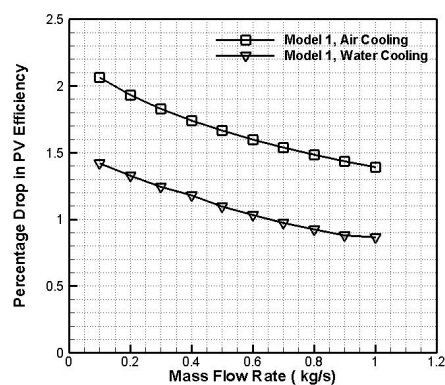


Figure 9. Effect of the mass flow rate of flowing fluid in percentage drop in PV cell efficiency for Model 1. $T_{amb} = 25^{\circ}\text{C}$.

The required TSC efficiency, namely, to have the same output electrical power as the output electrical power of the standalone PV cell when using water, is higher than using air or without cooling. That is because the drop in PV efficiency is the lowest, as shown in Figure 10. When using air or without cooling, the difference in the output electrical power between the standalone and the integrated PV is low, which means low η_{TSC} needs to cover this difference.

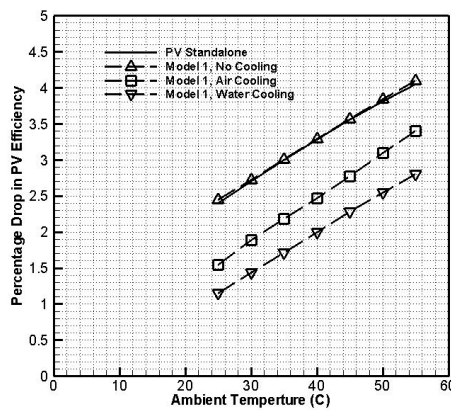
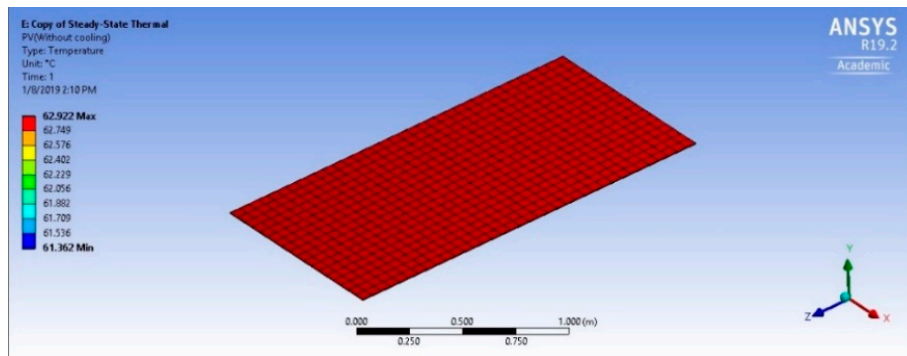


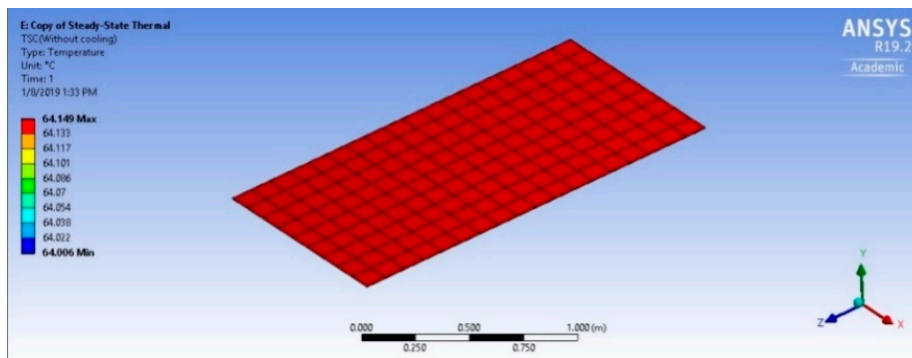
Figure 10. Effect of ambient temperature in percentage drop of PV efficiency of Model 1 and the standalone PV [36]. Mass flow rate = 0.5 kg/s.

According to the remarks from the previous figures, it is obvious that air or water flow through a single fluid duct below the conventional PV is not enough for cooling the solar model to its optimum operating temperature. For that reason, power production will be low. Another proposed model is to have another cooling space between the conventional PV cell and the TSC, beside the space under the PV cell. This can provide a higher heat transfer rate for both cells, causing the temperature of the cells to drop significantly.

Comparing the results in Figure 11 to that in Figure 4, it is clear that the temperature of both cells dropped significantly. Therefore, this suggested modification of using cooling fluid in the space between the PV and the TSC cell has improved the model. This can decently increase the convective heat transfer coefficient and thus lower the temperature of the cell, as shown in Figure 12.



(a)



(b)

Figure 11. Temperature contours (°C) of Model 2 without cooling: (a) PV cell; (b) TSC cell.

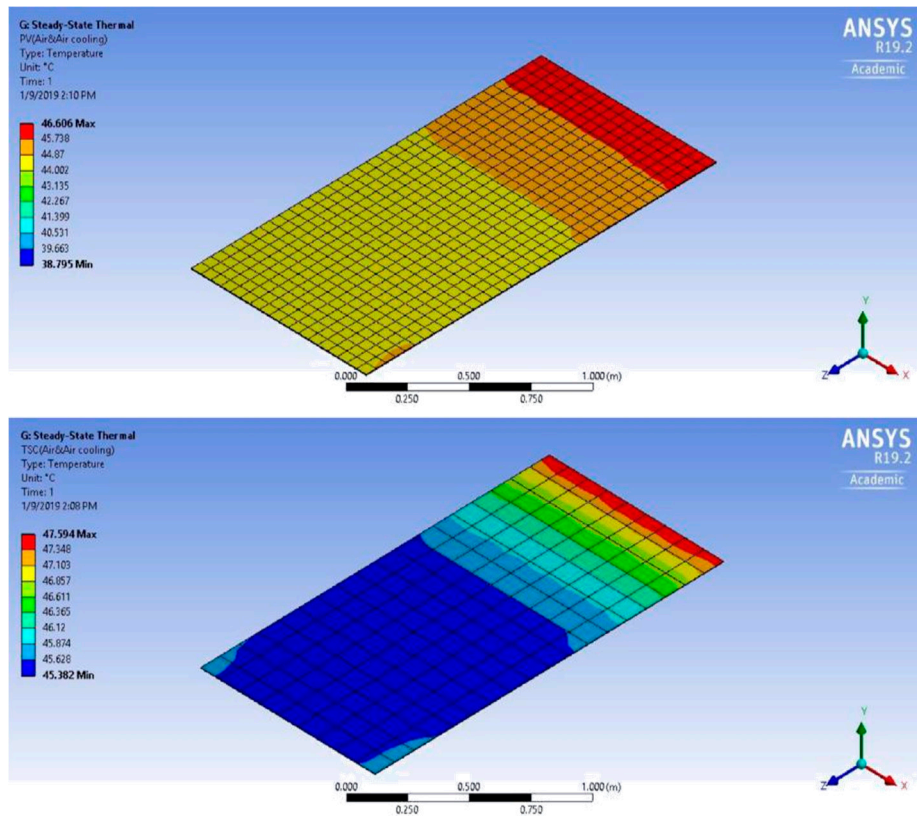


Figure 12. Temperature contours (°C) of Model 2 with air–air cooling. Top: PV cell; bottom: TSC cell.

Using water as a cooling fluid in the bottom space instead of air, while maintaining airflow in the fluid duct between the two solar cells, can produce a noticeable improvement in the results on the PV cell’s surface temperature. However, the TSC cell temperature will not be affected as much since the fluid is in direct contact with the bottom surface of the PV cell. Figure 13 shows the PV cell’s temperature distribution.

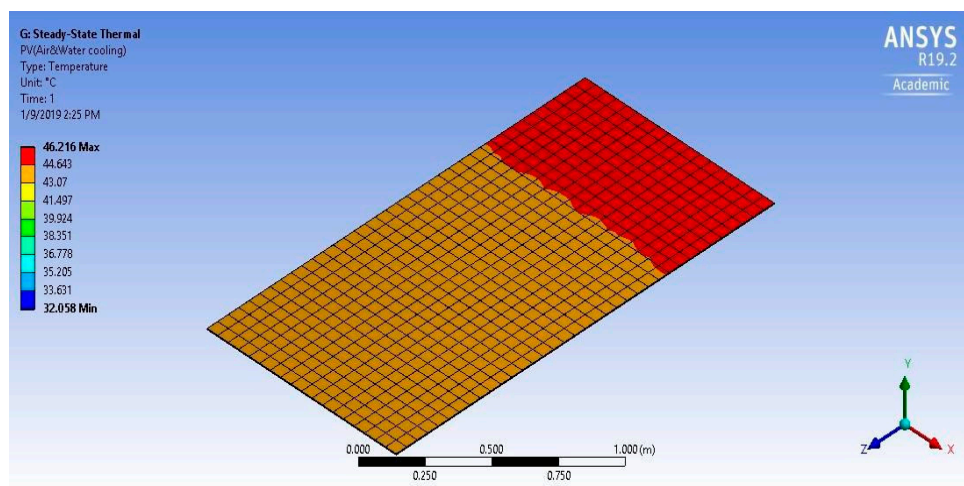


Figure 13. Temperature contours (°C) of Model 2 with air–water cooling of the PV cell.

A comparison of the maximum and minimum temperatures of the proposed Model 2 is shown in Table 4. As well known, increasing PV temperature will decrease PV efficiency. Therefore, PV cell

temperature must be reduced to increase PV cell efficiency. As such, Model 2 is a good model as it compares with Model 1 or a conventional PV cell.

It is important to mention that conventional PV cell efficiency is set to 15%. However, this efficiency can be obtained if the cell operates under optimum conditions, including a surface temperature of the cell of about 25 °C. When it comes to real-life conditions, the surface temperature is a bit far from the optimum one, which will have reduced efficiency when compared with that of a PV cell at a temperature of 25 °C. Moreover, the mass flow rate of the cooling fluid can still play an important role in the cooling process, where lower temperatures can be achieved with higher velocities or higher mass flow rates. As such better efficiency can be obtained, a comparison of the percentage drop in PV efficiency at the ambient temperature of 25 °C for Models 1 and 2 is shown in Figure 14.

Table 4. The maximum and minimum temperature values of the PV and TSC cells of Model 2.

$T_{\max, s \text{ tan dalone}} = 69.41 \text{ } ^\circ\text{C}$; $T_{\min, s \text{ tan dalone}} = 65.63 \text{ } ^\circ\text{C}$.

Temperature °C	Cell	Standalone PV [36]	Without Cooling	Air—Air Cooling	Air—Water Cooling
Maximum Temperature (°C)	PV Cell	69.45	62.92	46.74	46.64
	TSC Cell	–	64.15	47.35	47.59
Minimum Temperature (°C)	PV Cell	65.10	61.54	39.66	33.63
	TSC Cell	–	64.02	45.63	45.64

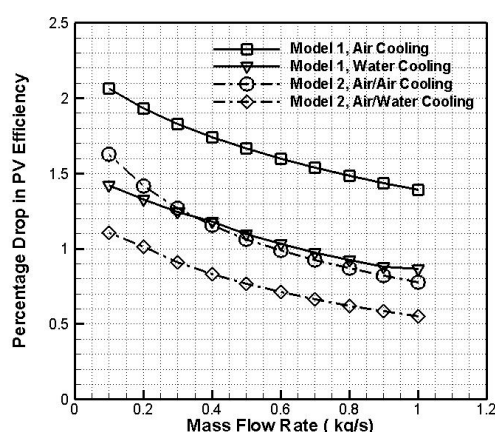


Figure 14. Comparison of the percentage drop in PV efficiency for Models 1 and 2 for different mass flow rates. $T_{\text{amb}} = 25 \text{ } ^\circ\text{C}$.

For the TSC, the required efficiency just to have the same output power as the standalone PV will increase with the increase in mass flow rate, as shown in Figure 15. Since increasing the mass flow rate will achieve higher PV efficiency, based on Equation (21), the required efficiency of the TSC must increase as well.

Figure 16 shows the effect of the ambient temperature on the required TSC efficiency just to have the same output power as the standalone PV of Model 2 and provides a comparison with Model 1. High ambient temperature results in low overall power.

Moreover, the ambient temperature can play a major role in dropping the efficiency, as shown in Figure 17. From this figure, the percentage drop in PV efficiency drops down with an increase in ambient temperature. This parameter can contribute to selecting the required PV; therefore, Figure 17 shows different ranges of temperature through which PV efficiency can change. It is important to note that with different ambient temperatures, the selection of the transparent solar cell will differ since the PV efficiency will vary. Additionally, Figure 17 shows a comparison of the percentage drop in PV cell efficiency for the standalone PV with Models 1 and 2. This figure shows that the best model is Model 2

with air–water cooling. Moreover, this figure shows validation for this study. The result of Model 1 without cooling is consistent with the result of the standalone PV, which provides verification of the proposed model. In addition, this figure shows the validation of the present model since the results of the standalone PV are in good agreement with Model 1 without cooling.

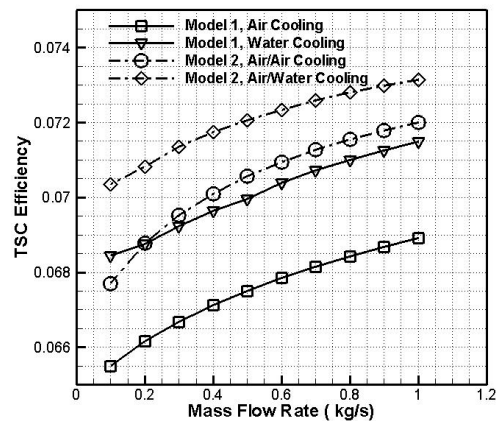


Figure 15. Comparison of TSC efficiency of Models 1 and 2 for different mass flow rates. $T_{amb} = 25\text{ }^{\circ}\text{C}$.

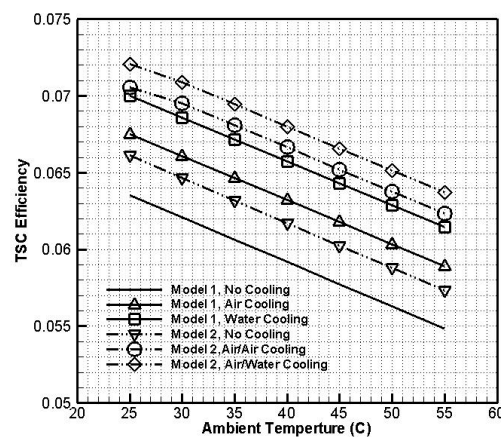


Figure 16. Comparison of TSC efficiency of Model 2 and Model 1 for different ambient temperatures. Mass flow rate = 0.5 kg/s; transparency = 0.75.

It is important to indicate that the TSC will block a small portion of the sun rays that the conventional PV cell will receive. This means that choosing an appropriate TSC to be integrated with the conventional PV cell is very important. In order to optimize the integration of the TSC with a traditional PV cell, three parameters should be taken into account in this model. According to Equation (21), the parameters are TSC transparency, TSC efficiency, and PV cell efficiency. Figure 18 shows the efficiency of the TSC with the transparency of the cell for different PV efficiency rates. This figure indicates the values of TSC transparency and efficiency that must be used with the conjugate efficiency of the conventional PV cell to achieve an optimum integration of TSCs with PV cells.

The previous results indicate that Model 1 without flowing fluid is considered to be a poor thermal model. For example, Figures 7 and 16 show the relationship between the required TSC efficiency in order to have the same output power as the standalone PV and the ambient temperature. The TSC has an efficiency of 0.07 for the first model, while the second model has an efficiency of 0.073 with water cooling at an ambient temperature of 25 °C. The difference might not be that large, but it certainly affects the efficiency of the conventional PV as well.

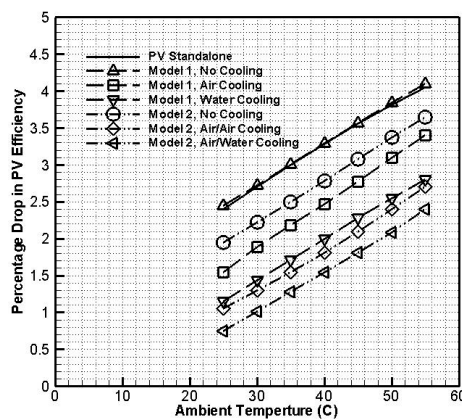


Figure 17. Comparison of the percentage drop in PV efficiency for Model 1, Model 2, and the standalone PV cell [36]. Mass flow rate = 0.5 kg/s, transparency = 0.75.

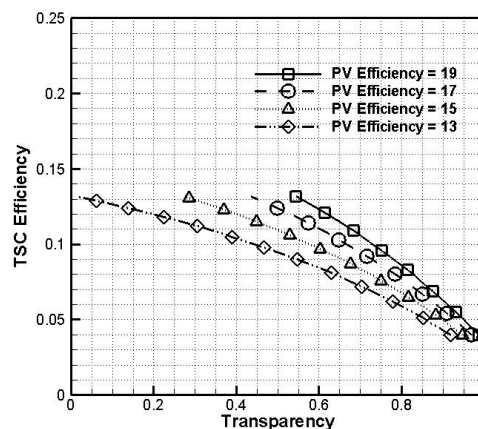


Figure 18. TSC efficiency vs. transparency for different PV efficiency rates.

It is obvious that Figure 10 has a higher slope, which means lower PV efficiency since the y -axis represents the absolute difference between the optimum efficiency and the resultant efficiency. Using the same logic, we observe from Figure 14 that the slope is more decaying compared to Figure 9, which indicates that PV efficiency will get closer to the optimum efficiency as the flow rate of the fluid increases in Model 2, rather than in Model 1.

The minimum TSC efficiency just to have the same output of electrical power as the standalone PV, at 75% transparency and 25 °C ambient temperature, without cooling, is equal to 0.063519 for Model 1 and 0.066119 for Model 2. Note that the efficiency needed in Model 2 is higher than that in Model 1 because the space between the TSC and the PV in Model 2 means better cooling. Then, the output of electrical power of the PV will be higher and the required TSC efficiency just to have the same output of electrical power as the standalone PV will be higher.

5. Validations

The proposed model was validated by comparing the results of the standalone PV that were available in the literature [36] with the two models that are proposed in this paper. Tables 3 and 4 show the results of the maximum and minimum temperatures of the standalone PV with Model 1 and Model 2 without cooling. The results are in good agreement. Additionally, Figures 10 and 17 show the percentage drop in the voltage of the standalone PV with the present models. The results of the standalone PV are in good agreement with the present models without cooling.

6. Conclusions

In this paper, integrating a transparent solar cell with a conventional PV cell (TSC/SC) was theoretically proposed, simulated, and analyzed. This study does not take any economic aspects into consideration and these aspects will be the focus of an upcoming study after commercializing the transparent cell. The objective of this research is to achieve higher electrical and thermal efficiencies than with conventional PVs. The results showed that integrating a transparent solar cell with a conventional photovoltaic cell (TSC/SC) enabled the system to absorb and utilize both wavelengths of the solar radiation spectrum; the ultraviolet, infrared, and visible light spectrum. Although adding the transparent solar cell was supposed to increase the output energy due to the utilization of the unconverted solar radiation, at the same time, it had two negative side effects. The first effect was reducing the transmitted radiation to the conventional solar cell due to the transmissivity of the transparent cell. The second effect was increasing the conventional cell temperature due to the additional thermal resistance, which reduced the effectiveness of the cooling of the cell, so integrating TSC and SC is not always beneficial. To summarize, this paper investigated the operating and design conditions under which integrating a transparent solar cell with a conventional photovoltaic cell (TSC/SC) could harvest more electrical power from the same incident solar radiation. This is because the integration has positive core effects and negative side effects. In this study, the conditions under which the positive core effects offset the negative side ones were investigated. Additionally, the results showed that providing space between the TSC and the traditional PV cell avoided overheating both solar cells. Moreover, the transparency limitations, combined with the required efficiencies, are displayed mathematically and graphically. Furthermore, the effect of ambient temperature, mass flow rate, and fluid type in model efficiency was studied.

It is an initial theoretical study that shows some first results; it is almost a work in progress. In future works, the viability of the physical construction of the proposed models will be demonstrated, as well as an economic study that shows the cost of this new technology.

The findings of this study are as follows:

- Model 1:
 - 1- The required TSC efficiency just to have the same output power as the standalone PV increases as the ambient air temperature decreases and as the mass flow rate of the coolant increases.
 - 2- In general, the cooling process improved the efficiency of the PV. Using water as a coolant improved its efficiency more than air. The efficiency of the PV with mass flow rate = 0.5 kg/s and 25 °C as the ambient temperature was as follows: 0.067 for air cooling and 0.07 for water cooling.
 - 3- The percentage drop in PV cell efficiency decreases as the mass flow rate of the coolant increases and as the ambient temperature decreases, and it had the lowest value when water was used as a coolant. The percentage drop in PV efficiency was 1.4, with 25 °C as the ambient temperature and 1 kg/s mass flow rate of air, while it was 0.9 for water cooling. For 0.5 kg/s with the same temperature, it was 1.7 for air cooling and 1.1 for water cooling.
 - 4- The maximum and minimum temperatures of the PV cell were higher for the PV cell without cooling, and they were lower for this model with cooling. The maximum temperatures of the PV were as follows: 70.20, 63.14, and 53.66 °C, without cooling, with air cooling, and with water cooling, respectively. For the minimum temperatures, they were 64.90, 24.96, and 24.96 °C, without cooling, with air cooling, and with water cooling, respectively.
- Model 2:
 - 1- The percentage drop in PV cell efficiency decreases as the mass flow rate of the coolant increases and as the ambient temperature decreases, and it had the lowest value when air/water was used for cooling.

- 2- The required TSC efficiency, just to have the same output power as the standalone PV, increases as the mass flow rate increases and the ambient temperature decreases, and it had the highest value when air/water was used for cooling.
- 3- The maximum and minimum temperatures of the PV cell and the TSC were lower than that of Model 1, which means higher efficiency, as shown in Table 4.
- 4- The required TSC efficiency, just to have the same output power as the standalone PV, increases as the transparency decreases; to have higher efficiency, the PV efficiency should be higher with low transparency. For 13% PV efficiency, when the transparency = 0.2, the TSC efficiency was 12.0%, while it was 8.5% when transparency = 0.6.
- 5- Higher PV efficiency can be achieved by enhancing the cooling process by using two spaces: one between the TSC and the PV cell and the second at the bottom of the PV cell.
- 6- Adding the transparent solar cell was supposed to increase the harvested energy due to the utilization of the unconverted solar radiation. However, it left two negative side effects. The first negative side effect was the reduction of the transmitted radiation to the conventional solar cell due to the transmissivity of the transparent cell. The second negative side was increase in the conventional cell temperature due to the additional thermal resistance that reduced the effectiveness of cooling the cell from above.

Author Contributions: M.A.-N.: Conceived and designed the idea of this work. Supervised this work. Encouraged all to investigate and supervised the findings of this work. A.M.: providing the system description and the thermal model. Write governing equations. Performed the analytical calculations and the numerical simulations. B.A.-B.: collecting the data, and writing mathematic equations, providing reliable data regarding the transparent PV cells technology through research, analysis and writing the article's script. K.A.K.: Provide the validation of this study, help in performed the analysis and extracting some of the figures, improve the discussion and the conclusion section, review the paper with input from all authors. All authors are discussed the results and contributed to the final manuscript. All authors have read and agreed to the published version of the manuscript.

Funding: This research received no external funding.

Conflicts of Interest: The authors declare no conflict of interest.

Nomenclature

C_p	Specific heat ratio (J/kg K)
dz	Element length in the flow direction
P	Generated electrical power (W/m ²)
G	Incident solar radiation (W/m ²)
h	Convection heat transfer coefficient at the bottom of the PV in model 1, (W/m ² K)
h_1	Convection heat transfer coefficient at the bottom of the TSC in model 2, (W/m ² K)
h_2	Convection heat transfer coefficient at the top of the PV in model 2, (W/m ² K)
h_3	Convection heat transfer coefficient at the bottom of the PV in model 2, (W/m ² K)
h_{rd}	Radiation heat transfer coefficient between the bottom of the PV and the surface of the insulation material, (W/m ² K)
h_4	Convection heat transfer coefficient at the insulation surface in model 2, (W/m ² K)
h_{rg}	Radiation heat transfer coefficient between the TSC and the sky, (W/m ² K)
h_w	Convection heat transfer coefficient of the wind, (W/m ² K)
k_{PV}	Thermal conductivity of the PV, (W/m K)
k_o	Thermal conductivity of organic TSC, (W/m K)
L	Model length, (m)
L_o	Thickness of organic TSC, (m)
L_{PV}	Thickness of the PV, (m)
\dot{m}	Mass flow rate, (kg/s)
PV	Photovoltaic
Q	Amount of the useful heat (W)

q_{th1}	Heat generation rate on the surface of the TSC, (W/m ²)
q_{th2}	Heat generation rate on the surface of the PV cell, (W/m ²)
q_u	Rate of thermal energy absorbed per unit area at the bottom of PV cell in model, (W/m ²)
q_{u1}	Rate of thermal energy absorbed per unit area of the TSC by the fluid in the upper fluid duct in model 2(W/m ²)
q_{u2}	Rate of thermal energy absorbed per unit area of the PV by the fluid in the lower fluid duct in model 2 (W/m ²)
TSC	Transparent solar cell
T_{fo}	Organic TSC front temperature, (K)
T_{bo}	TSC bottom surface temperature, (K)
T_{bs}	PV cell bottom temperature, (K)
T_{f2}	Mean temperature of the fluid inside the lower duct between the bottom of the PV and the insulation material, (K)
T_i	Temperature of insulation material, (K)
T_{f1}	Mean temperature of the fluid inside the upper duct between the front of the PV and the TSC, (K)
T_{fs}	PV front surface temperature, (K)
U_{ex1}	Overall heat transfer coefficient of the top side, (W/m ² K)
U_{ex2}	Overall heat transfer coefficient of the bottom side, (W/m ² K)
V_w	Wind speed (m/s)
W	Model width (m)
Greek	
α	Absorptivity
ε_1	Emissivity of the PV
ε_2	Emissivity of the insulation material
τ	Transmissivity
η	Efficiency
σ	Stefan- Boltzmann constant, (W/m ² K ⁴)
ξ	Percentage of the visible light

References

1. Tak, S.; Woo, S.; Park, J.; Park, S. Effect of the changeable organic semi transparent solar cell window on building energy efficiency and user comfort. *Sustainability* **2017**, *9*, 950. [\[CrossRef\]](#)
2. Alfegi, E.M.A.; Sopian, K.B.; Othman, M.Y.; Yatim, B.B. Mathematical model of double pass photovoltaic thermal air collector with fins. *Am. J. Environ. Sci.* **2009**, *5*, 592–598. [\[CrossRef\]](#)
3. McEvoy, A.; Markvart, T.; Castaner, L. *Practical Handbook of Photovoltaic: Fundamentals and Applications*, 1st ed.; Elsevier: Oxford, UK, 2003.
4. Szlufcik, J.; Sivoththaman, S.; Nlis, J.F.; Mertens, R.P.; Van Overstraeten, R. Low-cost industrial technologies of crystalline silicon solar cells. *Proc. IEEE* **1997**, *85*, 711–730. [\[CrossRef\]](#)
5. Xi, Z.; Yang, D.; Dan, W.; Jun, C.; Li, X.; Que, D. Texturization of cast multicrystalline silicon for solar cells. *Semicond. Sci. Technol.* **2004**, *19*, 485. [\[CrossRef\]](#)
6. Song, J.-H.; An, Y.-S.; Kim, S.-G.; Lee, S.-J.; Yoon, J.; Choung, Y.-K. Power output analysis of transparent thin-film module in building integrated photovoltaic system (BIPV). *Energy Build* **2008**, *40*, 2067–2075. [\[CrossRef\]](#)
7. Moharram, K.A.; Abd-Elhady, M.S.; Kandi, H.A.; El-Sherif, H. Enhancing the performance of photovoltaic panels by water cooling. *Ain Shams Eng. J.* **2013**, *4*, 869–877. [\[CrossRef\]](#)
8. Alonso García, M.C.; Balenzategui, J.L. Estimation of photovoltaic module yearly temperature and performance based on nominal operation cell temperature calculations. *Renew. Energy* **2010**, *29*, 1997–2010. [\[CrossRef\]](#)
9. Lunt, R.R.; Bulović, V. Transparent, near-infrared organic photovoltaic solar cells for window and energy-scavenging applications. *Appl. Phys. Lett.* **2011**, *98*, 113305. [\[CrossRef\]](#)
10. Yoon, S.; Tak, S.; Kim, J.; Jun, Y.; Kang, K.; Park, J. Application of transparent dye-sensitized solar cells to building integrated photovoltaic systems. *Build. Environ.* **2011**, *46*, 1899–1904. [\[CrossRef\]](#)

11. Suzuoki, Y.; Cai, G.; TeruyoshiMizutani and Masayuki Ieda. TSC study on interfacial phenomena in PE (Polyethylene)-EVA (Ethylene-Vinylacetate Copolymer) laminated films. *Jpn. J. Appl. Phys.* **1982**, *21*. [[CrossRef](#)]
12. Husain, A.A.F.; Hasan, W.Z.W.; Shafie, S.; Hamidon, M.N.; Pandey, S.S. A review of transparent solar photovoltaic technologies. *Renew. Sustain. Energy Rev.* **2018**, *94*, 779–791. [[CrossRef](#)]
13. Da, Y.; Xuan, Y.; Li, Q. From light trapping to solar energy utilization: A novel photovoltaic–thermoelectric hybrid system to fully utilize solar spectrum. *Energy* **2015**, *95*, 200–210. [[CrossRef](#)]
14. Karima, E.; Amori, K.; Taqi Al-Najjar, H.M. Analysis of thermal and electrical performance of a hybrid (PV/T) air based solar collector for Iraq. *Appl. Energy* **2012**, *98*, 384–395. [[CrossRef](#)]
15. Hosenuzzaman, M.; Rahim, N.A.; Selvaraj, J.; Hasanuzzaman, M.; Malek, A.B.M.A.; Nahar, A. Global prospects, progress, policies, and environmental impact of solar photovoltaic power generation. *Renew. Sustain. Energy Rev.* **2015**, *41*, 284–297. [[CrossRef](#)]
16. Zeng, K.; Zhu, F.; Hu, J.; Shen, L.; Zhang, K.; Gong, H. Investigation of mechanical properties of transparent conducting oxide thin films. *Thin Solid Film.* **2003**, *443*, 60–65. [[CrossRef](#)]
17. Shukla, A.K.; Sudhakar, K.; Baredar, P. Design, simulation and economic analysis of standalone roof top solar PV system in India. *Solar Energy* **2016**, *136*, 437–449. [[CrossRef](#)]
18. Betancur, R.; Romero-Gomez, P.; Martinez-Otero, A.; Elias, X.; Maymó, M.; Martorell, J. Transparent polymer solar cells employing a layered light-trapping architecture. *Nat. Photonics* **2013**, *7*, 995–1000. [[CrossRef](#)]
19. Tyagi, V.V.; Rahim, N.A.A.; Rahim, N.A.; Selvaraj, J.A.L. Progress in solar PV technology: Research and achievement. *Renew. Sustain. Energy Rev.* **2013**, *20*, 443–461. [[CrossRef](#)]
20. Sarhaddi, F.; Farahat, S.; Ajam, H.; Behzadmehr, A.; Mahdavi, A.M. An improved thermal and electrical model for a solar photovoltaic thermal (PV/T) air collector. *Appl. Energy* **2010**, *87*, 2328–2339. [[CrossRef](#)]
21. Park, K.E.; Kang, G.H.; Kim, H.I.; Yu, G.J.; Kim, J.T. Analysis of thermal and electrical performance of semi-transparent photovoltaic (PV) module. *Energy* **2010**, *35*, 2681–2687. [[CrossRef](#)]
22. Pucar, M.D.J.; Despic, A.R. The enhancement of energy gain of solar collectors and photovoltaic panels by the reflection of solar beams. *Energy* **2002**, *27*, 205–223. [[CrossRef](#)]
23. Karthick, A.; KalidasaMurugavel, K.; Kalaivani, L. Performance analysis of semitransparent photovoltaic module for skylights. *Energy* **2018**, *162*, 798–812. [[CrossRef](#)]
24. Wang, Y.; Li, Q.; Li, D.; Hong, H. Thermodynamic analysis for a concentrating photovoltaic photothermochemical hybrid system. *Energy* **2018**, *148*, 528–536. [[CrossRef](#)]
25. Schiro, F.; Benato, A.; Stoppato, A.; Destro, N. Improving photovoltaics efficiency by water cooling: Modelling and experimental approach. *Energy* **2017**, *137*, 798–810. [[CrossRef](#)]
26. Yin, E.; Li, Q.; Xuan, Y. A novel optimal design method for concentration spectrum splitting photovoltaic–thermoelectric hybrid system. *Energy* **2018**, *163*, 519–532. [[CrossRef](#)]
27. Al-Nimr, M.A.; Bukhari, M.; Mansour, M. A combined CPV/T and ORC solar power generation system integrated with geothermal cooling and electrolyser/fuel cell storage unit. *Energy* **2017**, *133*, 513–524. [[CrossRef](#)]
28. Li, G.; Shittu, S.; Ma, X.; Zhao, X. Comparative analysis of thermoelectric elements optimum geometry between photovoltaic thermoelectric and solar thermoelectric. *Energy* **2019**, *171*, 599–610. [[CrossRef](#)]
29. Muthu Manokar, A.; Prince Winston, D.; Kabeel, A.E.; Sathyamurthy, R. Sustainable fresh water and power production by integrating PV panel in inclined solar still. *J. Clean. Prod.* **2018**, *172*, 2711–2719. [[CrossRef](#)]
30. BanyMousa, O.; Kara, S.; Taylor, R.A. Comparative energy and greenhouse gas assessment of industrial rooftop-integrated PV and solar thermal collectors. *Appl. Energy* **2019**, *241*, 113–123. [[CrossRef](#)]
31. Katsura, T.; Radwan, A.; Yang, Z.; Nakamura, M.; Nagano, K. Energy conservation using new structured-core and transparent vacuum insulation panels: Numerical simulation with experimental validation. *Sol. Energy* **2019**, *193*, 885–905. [[CrossRef](#)]
32. Alrashidi, H.; Ghosh, A.; Issa, W.; Sellami, N.; Mallick, T.K.; Sundaram, S. Thermal performance of semitransparentCdTe BIPV window at temperate climate. *Sol. Energy* **2020**, *195*, 536–543. [[CrossRef](#)]
33. Cengel, Y.A.; Boles, M.A. *Thermodynamics: An Engineering Approach*, 5th ed.; McGraw-Hill Science: New York, NY, USA, 2005.
34. Ozisk, M.N. *Heat Transfer, Basic Approach*; McGraw-Hill: New York, NY, USA, 1985.

35. Incropera, F.P.; Dewitt, D.P.; Bergman, T.L.; Lavane, A.S. *Principles of Heat and Mass Transfer*, 7th ed.; Jonn Wiley and Sons: Hoboken, NJ, USA, 2013.
36. Zubeer, S.; Mohammed, H.; Ilkan, M. A review of photovoltaic cells cooling techniques. *E3S Web Conf.* **2017**, *22*, 00205. [[CrossRef](#)]



© 2020 by the authors. Licensee MDPI, Basel, Switzerland. This article is an open access article distributed under the terms and conditions of the Creative Commons Attribution (CC BY) license (<http://creativecommons.org/licenses/by/4.0/>).